Atmos. Meas. Tech., 18, 7221–7230, 2025 https://doi.org/10.5194/amt-18-7221-2025 © Author(s) 2025. This work is distributed under the Creative Commons Attribution 4.0 License.





# High-purity nitrous acid (HONO) generation and quantification using broadband cavity-enhanced absorption spectroscopy (BBCEAS)

Alexis P. Harper<sup>1</sup>, Callum E. Flowerday<sup>1</sup>, Zachary Giauque<sup>1</sup>, Kaitlyn Brewster<sup>1</sup>, Ryan Thalman<sup>2</sup>, and Jaron C. Hansen<sup>1</sup>

Correspondence: Jaron C. Hansen (jchansen@byu.edu)

Received: 26 August 2025 – Discussion started: 29 September 2025

Revised: 10 November 2025 – Accepted: 11 November 2025 – Published: 2 December 2025

Abstract. Nitrous acid (HONO) is a key atmospheric precursor to hydroxyl radicals (OH), which drive oxidation processes in the troposphere. Accurate quantification of HONO is essential for modelling atmospheric chemistry but is often challenging due to low ambient concentrations, significant wall losses from instruments with inlets, and interference from co-produced nitrogen dioxide (NO2). Laboratory generation methods frequently struggle to produce HONO in both high purity and usable quantities. This study introduces a simple, scalable method for generating high-purity HONO relative to NO<sub>2</sub> via the reaction of hydrochloric acid (HCl) and sodium nitrite (NaNO<sub>2</sub>) in a multi-bubbler system. The method incorporates a thermal "catch and release" mechanism to selectively trap HONO and separate it from NO2 prior to analysis. While the melting point of NO<sub>2</sub> is wellestablished at -9 °C, the melting point of HONO was monitored and determined to be -4 °C, enabling the thermal separation mechanism to function effectively. Broadband cavityenhanced absorption spectroscopy (BBCEAS) was used for detection and quantification in the 329-344 nm region. Systematic optimization of bubbler temperatures, carrier gas flow rates, capture durations, and moisture levels yielded HONO purities greater than 96 %. This method enables reliable and flexible production of high-purity HONO relative to NO<sub>2</sub>, making it well-suited for use in laboratory-based chamber studies and instrument calibration applications.

# 1 Introduction

Nitrous acid (HONO) plays a pivotal role in atmospheric chemistry due to its photolysis at or below 579 nm, producing hydroxyl radicals (OH) via Reaction (R1), which initiate oxidation processes in the troposphere (Burkholder et al., 2020; Cox et al., 1976a). At lower wavelengths, less than 362 nm, HONO photolyzes to produce NO<sub>2</sub> via Reaction (R2), which also contributes to oxidative processes in the troposphere (Burkholder et al., 2020).

$$HONO + hv (< 579 \text{ nm}) \longrightarrow OH + NO$$
 (R1)

$$HONO + hv (< 362 \text{ nm}) \longrightarrow H + NO_2$$
 (R2)

HONO is introduced into the atmosphere both through direct emissions and secondary formation. Primary emissions occur from combustion processes such as biomass burning, industrial burning, domestic heating, and internal combustion engines (Pitts et al., 1984; Kurtenbach et al., 2001; Xu et al., 2015). Secondary atmospheric HONO formation involves heterogeneous reactions, including the hydrolysis of NO<sub>2</sub> on humid surfaces (Finlayson-Pitts et al., 2003) and NO2 reduction by adsorbed hydrocarbons (Gutzwiller et al., 2002), as well as homogeneous gas-phase reactions and photolysis of gaseous nitrophenols. Su et al. (2011) identified soil microbial processes as a potential source of HONO through nitrite conversion. Additionally, in winter, HONO concentrations can be enhanced due to increased photolysis of nitrate in snowpacks and the presence of temperature inversions, which trap pollutants near the surface, decrease ver-

<sup>&</sup>lt;sup>1</sup>Brigham Young University, Department of Chemistry and Biochemistry, Provo, UT 84602, USA

<sup>&</sup>lt;sup>2</sup>Snow College, Department of Chemistry, Richfield, UT 84701, USA

tical mixing, and extend the lifetime of precursors, promoting HONO formation pathways (Honrath et al., 2002; Beine et al., 2008; Michoud et al., 2014).

While HONO formation mechanisms vary by location, its atmospheric significance is consistently linked to its role in OH radical production. During daylight hours, HONO photolysis serves as a major source of OH, especially in the early morning when other photochemical sources like ozone (O<sub>3</sub>) and formaldehyde (HCHO) are less active (Kleffmann, 2007). OH radical governs atmospheric oxidative capacity and contributes to the degradation of pollutants, influencing the formation of ground-level ozone and photochemical smog, both hazardous to human health (Elshorbany et al., 2010). Numerous studies have quantified the relative contributions of various OH initiation pathways, showing that HONO plays a major role in the lower atmosphere, even outside of urban settings (Ren et al., 2003, 2006; Elshorbany et al., 2010; Dusanter et al., 2009). Due to its importance, a comprehensive understanding of HONO sources and behaviour is essential for accurately modelling atmospheric composition and predicting pollutant lifetimes.

Reliable detection and quantification of HONO remain challenging due to interference from other nitrogen oxides and its low ambient concentrations. Various techniques, including chemiluminescence (Kanda and Taira, 1990), laserinduced fluorescence (LIF) (Bottorff et al., 2021; Ning and Pfab, 1997), differential optical absorption spectroscopy (DOAS) (Febo et al., 1995), Fourier-transform infrared spectroscopy (FTIR) (Gingerysty and Osthoff, 2020), long path absorption photometry (LOPAP) (Heland et al., 2001; von der Heyden et al., 2022), cavity ring-down spectroscopy (CRDS) (Gingerysty and Osthoff, 2020), ultraviolet (UV) absorption (King and Moule, 1962; Stockwell and Calvert, 1978), and broadband cavity-enhanced absorption spectroscopy (BBCEAS) (Dixneuf et al., 2022; Gherman et al., 2008; Wu et al., 2012; Wu et al., 2014; Duan et al., 2018; Jordan and Osthoff, 2020), have been employed for HONO detection. Each method presents trade-offs in sensitivity, selectivity, and operational complexity.

In parallel, the generation of HONO in laboratory settings has been essential for calibrating instruments and simulating atmospheric processes. Traditional methods typically rely on acid displacement reactions, where a proton donor (e.g., H<sub>2</sub>SO<sub>4</sub>, HCl) reacts with a nitrite salt. However, existing methods often produce significant amounts of NO<sub>2</sub> alongside HONO, complicating spectral quantification, particularly for spectroscopic methods where spectral overlap occurs (King and Moule, 1962; Stockwell and Calvert, 1978; Cox and Derwent, 1976b). While some techniques achieve high-purity HONO, they often involve complex setups, such as the use of permeation devices, or yield low concentrations (Gingerysty and Osthoff, 2020; Lao et al., 2020; Reed et al., 2016; Villena and Kleffman, 2022).

Early generation methods, such as bubbling air through a solution of 0.1 M sodium nitrite with 1.4 %-2.5 % sulfu-

ric acid, produced HONO vapours with purities around 50 % (Cox and Derwent, 1976b). Subsequent strategies used oxalic acid sublimed onto sodium nitrite, achieving purities of 50%-90% depending on water content (Braman and De la Cantera, 1986). Flow reactor designs improved stability and control, achieving > 90% purity at low concentrations by dynamically mixing sulfuric acid with sodium nitrite (Taira and Kanda, 1990).

More recently, hydrochloric acid (HCl) has emerged as a viable proton donor for producing high-purity HONO via Reaction (R3).

$$HCl + NaNO_2 \longrightarrow HONO + NO_2 + NaCl$$
 (R3)

Febo et al. (1995) developed a permeation-based system where HCl vapour reacted with solid NaNO2 in a humidified gas stream, achieving HONO purities of 99.5 %. Other groups have refined this concept, though some reported that HONO concentrations must remain low to avoid disproportionation (Stutz et al., 2000). This study aims to address these limitations by presenting a simple and scalable method for generating HONO using HCl as the proton donor. By thermally separating HONO from NO2, the method achieves high purity relative to NO<sub>2</sub> while producing sufficient quantities for laboratory use and experimental applications. Beyond controlled environments, its simplicity, reproducibility, and scalability (up or down) make it suitable for integration into diverse analytical setups and for deployment in longterm atmospheric monitoring both in chamber setups and as standards and calibration sources for field monitoring sites.

### 2 Experimental

# 2.1 HONO generation setup

The experimental system, shown in Fig. 1, comprises a series of three bubblers immersed in controlled temperature baths. Nitrogen  $(N_2)$  serves as the carrier gas throughout the system, with tested flow rates ranging from 100–500 standard cubic centimetres per minute (SCCM). The first bubbler contains 12 M HCl, while the second houses a NaNO<sub>2</sub> slurry dispersed over 4 mm glass beads to maximize the surface area for the gas-phase reaction. These two bubblers are held in a constant temperature bath, with tested temperatures ranging from 20 to 40 °C. The third bubbler, the capture stage, contains dry 4 mm glass beads and is maintained in a separate temperature bath at tested temperatures ranging from -5 to -8 °C to condense and trap HONO.

Between the second and third bubblers, a condenser is set up to lower the gas mixture temperature before entering the collection bubbler. Antifreeze solution is introduced to the condenser from the collection bubbler temperature bath, making it the same temperature as the collection bubbler, which gives HONO time to cool and freeze at negative temperatures. A dilution manifold is situated between the HONO

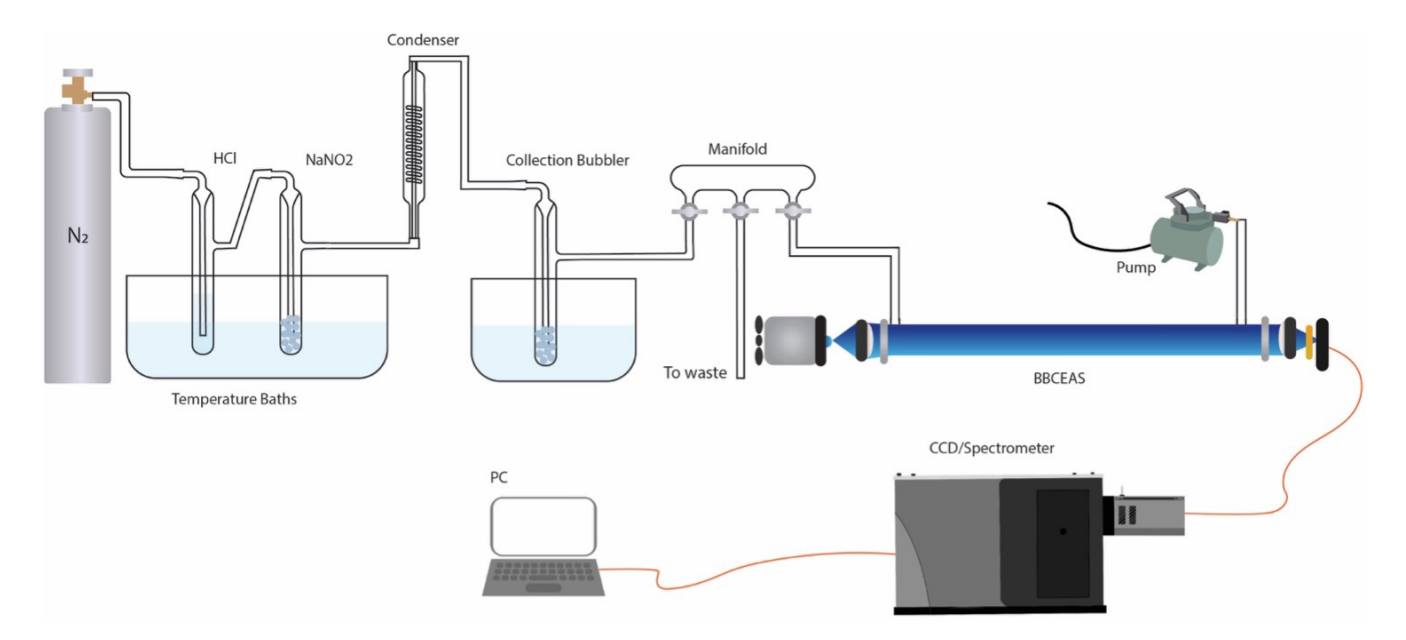


Figure 1. Nitrogen gas flows through the experimental system to produce  $NO_2$  and HONO. HONO is captured on the final bubbler's beads, while  $NO_2$  is passed through the manifold to waste. After the collection period, reactant bubblers are bypassed and the collection bubbler is heated up to release HONO, which flows through the BBCEAS cavity to be analysed.

generation system and the BBCEAS cavity. During the capture phase, the manifold is directed toward waste only, allowing NO<sub>2</sub> to escape, while HONO is captured on the bubbler's beads. After a 1 h reaction and capture phase, the HCl and NaNO<sub>2</sub> bubblers are bypassed, and nitrogen is introduced at a flow rate of 1 SLM. The capture bubbler is then gradually heated to 30 °C to release the trapped HONO for analysis. The manifold exit leading to the BBCEAS is then opened and allows the mixture to be diluted by a factor of two, ensuring the measured extinction falls within the instrument's linear response range and enabling accurate quantification. Adjusting the flow rate in this last step can alter the concentration of HONO exiting the system.

# 2.2 Thermal "catch and release" mechanism

The melting point of HONO was measured to optimize its selective capture. While the melting point of  $NO_2$  is well-established at  $-9\,^{\circ}\text{C}$  (O'Neil et al., 2013), HONO's melting point was identified by incrementally lowering the capture bubbler temperature and monitoring HONO release. This information guided the selection of capture temperatures that maximize HONO collection while minimizing  $NO_2$  interference.

### 2.3 HONO detection using BBCEAS

Broadband cavity-enhanced absorption spectroscopy (BBCEAS) has been used for detection of a wide range of molecules including short chained alcohols, formaldehyde, glyoxal (CHOCHO), methyl glyoxal (CH<sub>3</sub>COCHO) iodine

oxide (IO), water vapour (H<sub>2</sub>O), oxygen dimers (O<sub>4</sub>), sulphur dioxide (SO<sub>2</sub>), NO<sub>2</sub>, and OH radical. (Thalman and Volkamer, 2010; Washenfelder et al., 2016; Thalman et al., 2022; Flowerday et al., 2023a, b, 2025) Briefly, BBCEAS employs highly reflective mirrors (R > 99.9%) to form an optical cavity that amplifies a 1 m base pathlength to an effective sample pathlength of 2000 m. The cavity consists of two 1" planar-concave AR-coated mirrors (Layertec 109657) mounted 1 m apart within a carbon pultruded tube cage system (Goodwinds) using 3D-printed PLA brackets. The cavity is enclosed in a brass pipe sealed against the mirrors. The light source is a UV-LED centred at 340 nm (Roithner Lasertechnik, DUV340-SD353EL-31), mounted on a copper heat sink. A Peltier cooler (Digi-Key 102-166-ND), sandwiched between the LED and heat sink and controlled by a precision temperature controller (Meerstetter TEC-1091), maintains the LED at  $15 \pm 0.1$  °C to ensure stable light intensity. A fan is mounted on the back of the heat sink for additional thermal management. Light is guided through the cavity using UV AR-coated collimating and focusing optics (ThorLabs). A  $340 \pm 13$  nm bandpass filter (Edmund Optics, 84092) ensures that only the desired wavelength reaches the fibre optic cable (Thorlabs BFL200HS02), which directs the light to a CCD detector cooled to -20 °C (SR-303i). For each experiment, 30 spectra with 2s integration times were accumulated to yield one spectrum per minute. The optical setup is shown in Fig. 2.

A closed cavity configuration was utilized for the BBCEAS, using a pump to pull the sample through the cavity at a rate of 2 SLM from the manifold. The known Rayleigh



**Figure 2.** The BBCEAS cavity is comprised of a broadband light source coupled into an optical cavity consisting of two highly reflective mirrors, increasing the pathlength of the light. The transmitted light is collected and directed into a spectrometer via an optical fibre, where it is dispersed and recorded using a CCD detector.

scattering of N<sub>2</sub> and He ( $\varepsilon_{\{Ray,N_2\}}(\lambda)$ ,  $\varepsilon_{\{Ray,He\}}(\lambda)$ ), along with the observed intensity drop between spectra ( $I_{N_2}(\lambda)$ ) and  $I_{\text{He}}(\lambda)$ ) and the distance between the mirrors  $(d_0)$ , were used to calculate the reflectivity of the mirrors  $(R(\lambda))$ , as seen in Eq. (1) and Fig. 3, by flowing these gasses through the cavity directly prior to the experiment. This reflectivity value, along with the intensity of the reference spectrum  $(I_0(\lambda))$  and the spectrum of interest  $(I(\lambda))$ , was then used to determine extinction coefficients ( $\epsilon(\lambda)$ ), as seen in Eq. (2), to which the known literature cross-sections of HONO and NO2 could be fit  $(\sigma_{[NO_2]}, \sigma_{[HONO]})$ . From these fits, a concentration of the species ([NO<sub>2</sub>], [HONO]) could be calculated using Eq. (3). Using a series of concentrations over time, a total amount of HONO captured, measured in nanomoles, was calculated for each experiment. Figure 4 shows the representative fit of experimental data to HONO and NO<sub>2</sub>, as well as the residuals from this fit.

$$R(\lambda) = 1 - \frac{\left\{ d_0 \left( \frac{\left\{ I_{\{N_2\}}(\lambda) \right\}}{\left\{ I_{\{He\}}(\lambda) \right\}} \right) \left( \varepsilon_{\{Ray, N_2\}}(\lambda) - \varepsilon_{\{Ray, He\}}(\lambda) \right) \right\}}{\left\{ 1 - \left( \frac{\left\{ I_{\{N_2\}}(\lambda) \right\}}{\left\{ I_{\{He\}}(\lambda) \right\}} \right) \right\}}, \quad (1)$$

$$\varepsilon(\lambda) = \left(\frac{\{1 - R(\lambda)\}}{\{d_0\}} + \varepsilon_{\{\text{Ray,Air}\}}(\lambda)\right) \left(\frac{\{I_0(\lambda) - I(\lambda)\}}{\{I(\lambda)\}}\right), \quad (2)$$

where  $I_0$  is the intensity of light in  $N_2$ , and I is the intensity of light in our target sample.

$$\varepsilon(\lambda) = \sigma_{\{NO_2\}}[NO_2] + \sigma_{\{HONO\}}[HONO] + polynomial...$$
 (3)

Fit residuals were consistently unstructured, white noise distributed around zero, and an order of magnitude or smaller lower than the fitted extinction of HONO which serves as an indication of a good fit. The 1 min limit of detection (LOD) calculated from this fit residual, while measuring both NO<sub>2</sub> and HONO, is  $6.56 \times 10^8$  molec. cm<sup>-3</sup> for HONO and  $4.94 \times 10^8$  molec. cm<sup>-3</sup> for NO<sub>2</sub>, which is at least 3 orders of magnitude below the concentrations measured in this experiment thus indicating confidence in the fit to the extinction. The fit is not stretched or shifted at all and, therefore, had negligible bias towards either species when trying to fit the other.

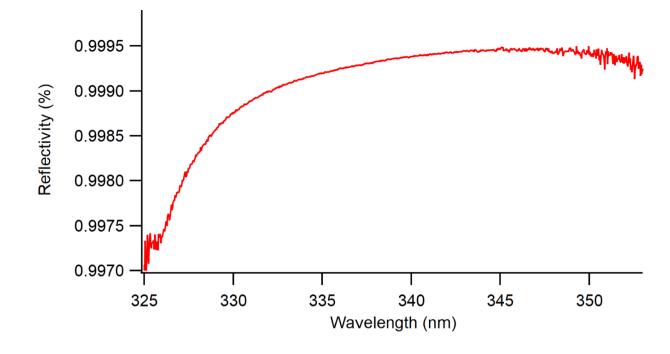


**Figure 3.** Reflectivity curve of mirrors. Mirrors are centered at 350 nm, where they peak at 99.95 % reflectivity and the light source emits with a maximum at 330 nm, resulting in the observed overlap. Absorbance is measured between 329 and 344 nm, where there was sufficient light and reflectivity for detection and sensitivity.

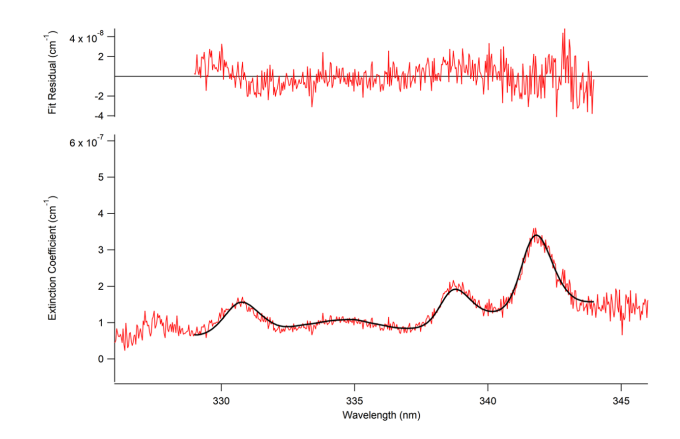


**Figure 4.** Fit of observed data (black) to the measured extinction coefficient (red) to determine the concentration of HONO and NO<sub>2</sub> in sample. Fit residual seen above.

The total  $1\sigma$  uncertainty in HONO and  $NO_2$  was determined by combining all independent sources of error, including uncertainties in temperature, cavity length, pressure, and the reported absorption cross-section uncertainties under these conditions of 5% for HONO (Bongartz et al., 1991) and 3% for  $NO_2$  (Vandaele et al., 1998). The total uncertainty was determined by combining the individual uncer-

tainties in quadrature to be  $3.5\,\%$  for  $NO_2$  and  $5.3\,\%$  for HONO.

### 3 Results and discussion

# 3.1 HONO melting point determination

The melting point of HONO was measured by monitoring its capture and subsequent release at decreasing bubbler bath temperatures. The first bath was kept constant at  $30\,^{\circ}\text{C}$  as HONO and NO<sub>2</sub> were being generated. The second temperature bath, containing the third bubbler, temperature was stepped down incrementally until the temperature of the bath reached  $-10\,^{\circ}\text{C}$ , which is below the known melting point of NO<sub>2</sub>. As seen in Fig. 5, below  $-4\,^{\circ}\text{C}$ , HONO recovery ceased, indicating this as the approximate melting point of HONO. NO<sub>2</sub>, by contrast, remained in the gas phase until the bath was cooled below  $-9\,^{\circ}\text{C}$ . This was beneficial as it is then possible to freeze out and capture HONO, as well as allow for the majority of NO<sub>2</sub> to pass through the capture bubbler due to the  $5\,^{\circ}\text{C}$  difference in melting points.

# 3.2 Capture bubbler optimization

Before attempting the use of the capture bubbler to further increase the purity of HONO being produced, initial tests without a capture stage yielded a HONO: NO2 ratio of 0.46:1  $(31.3 \pm 1.9\% \text{ purity})$ . This and following experiments kept a constant reactant bubbler bath temperature of 30 °C, containing the two bubblers with HCl and the NaNO2 slurry, and a flow rate of N<sub>2</sub> gas through the system set at 300 SCCM. To start, the capture bubbler bath was set to -8 °C, intending to allow any excess NO<sub>2</sub> to pass through the system before freezing out, while HONO adhered to the beads. Implementing a capture bubbler at -8 °C improved the ratio to 2.27:1  $(69.4 \pm 1.8 \%)$ . Further experiments raised the temperature of the capture bubbler bath incrementally to find an optimal temperature for HONO capture. As the temperature varied, the amount of HONO captured on the beads stayed relatively constant from -8 to -6 °C, while purities rose, meaning less NO₂ was being captured. Purity maximized at −5.5 °C  $(90.4 \pm 0.5 \%)$ , albeit with a slightly reduced HONO yield, decreasing from 41 to 37 nmol captured. Raising the temperature beyond -5.5 °C produced similar purity of HONO, but in smaller amounts, meaning less of both HONO and NO<sub>2</sub> were being captured on the beads. Figure 6 shows how purity and amount of HONO changed over different capture bubbler bath temperatures.

# 3.3 Reactant bubbler bath temperature optimization

Along with capture bubbler bath temperature, the reactant bubblers' bath temperature was also changed to determine optimal HONO synthesis conditions. Different reaction bubbler temperatures will prefer HONO or NO<sub>2</sub> production,

as temperature influences the reaction kinetics and chemical equilibria. In these experiments, the capture bubbler bath was kept constant at the optimal  $-5.5\,^{\circ}\text{C}$  and the flow rate remained at 300 SCCM. At 30 °C, the system produced the highest HONO purity (90.4  $\pm$  0.5 %), with the same ratio found above (9.44:1). Figure 7 shows how purity and amount of HONO changed over different reactant bubbler bath temperatures.

### 3.4 Carrier gas flow rate optimization

Lastly, the flow rate was varied to determine optimal HONO production. At lower flow rates, less HONO will be generated as less HCl gas is able to transfer to the second bubbler and react with NaNO2. However, once flow rates reach a certain point, N2 gas will be moving through the bubblers too fast to transfer HCl into the NaNO2 bubbler to be reacted. High flow rates also lead to NO<sub>2</sub> being pushed out of the NaNO<sub>2</sub> bubbler without being reacted. In these experiments, the optimal capture bubbler bath temperature of -5.5 °C and reactant bubbler bath temperature of 30 °C was used and the flow rate through the system was systemically varied. Flow rate experiments revealed an optimal value at 200 SCCM, yielding a HONO: NO<sub>2</sub> ratio of 25.53:1 (96.2  $\pm$  0.5 % purity). Flow rates below or above this value resulted in either insufficient reaction or excess NO2 breakthrough. Figure 8 shows how purity and amount of HONO varied with different flow rates. Figure 9 shows the concentration of HONO and NO<sub>2</sub> desorbed from the capture bubbler beads over time under optimal conditions of bubbler and capture temperatures, and carrier gas flow rate. Typically, it took 30–45 min for the glass beads to be completely desorbed of HONO and NO<sub>2</sub>. The more HONO and NO<sub>2</sub> collected, the longer the desorption process took.

### 3.5 Capture duration

HONO was collected on the beads of the final bubbler for 1 h in the general procedure, allowing for accurate comparison of different variables to optimize HONO production. However, extending the capture period from 1 to 2 h under optimal conditions resulted in a higher recovery of HONO (86 nmol) without compromising purity (95.0  $\pm$  0.6 % purity). Adjusting the collection time provides flexibility in generating specific HONO quantities. Additionally, because HONO remains stable when frozen on the beads, it can be stored for later use, allowing for controlled release from the generation system by modifying the flow rate.

### 3.6 Moisture sensitivity

The water content of the NaNO<sub>2</sub> slurry had a significant impact on product purity. Both saturated NaNO<sub>2</sub> solutions and dry solid NaNO<sub>2</sub> favoured increased NO<sub>2</sub> production, resulting in lower HONO purities compared to the slurry used under optimal conditions. In the optimal preparation, enough

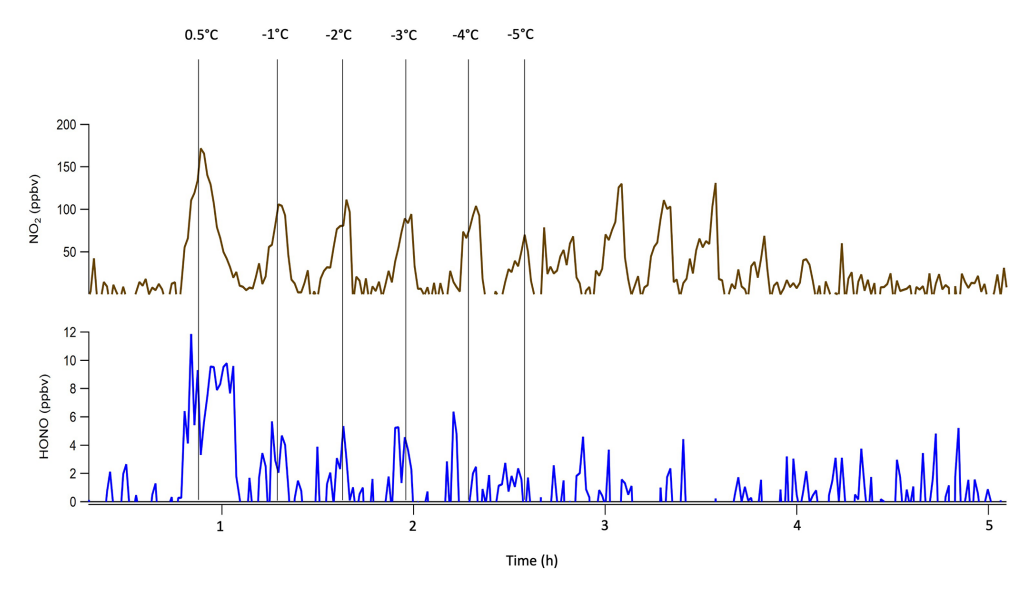
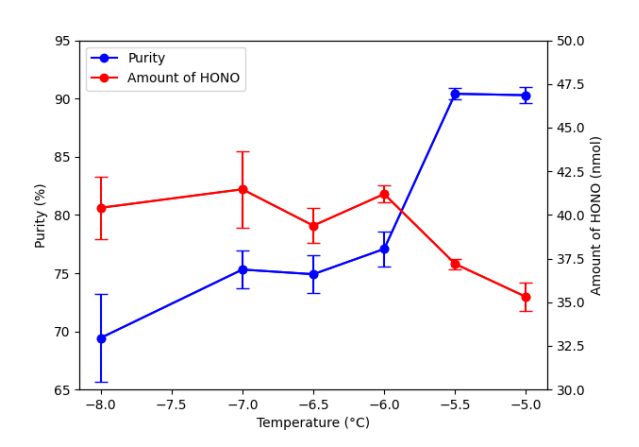


Figure 5. Concentration vs. time plot of  $NO_2$  (brown) and HONO (blue) as temperature is changed incrementally over time to determine the melting point of HONO.



**Figure 6.** Effect of capture bubbler bath temperature on purity and amount of HONO.

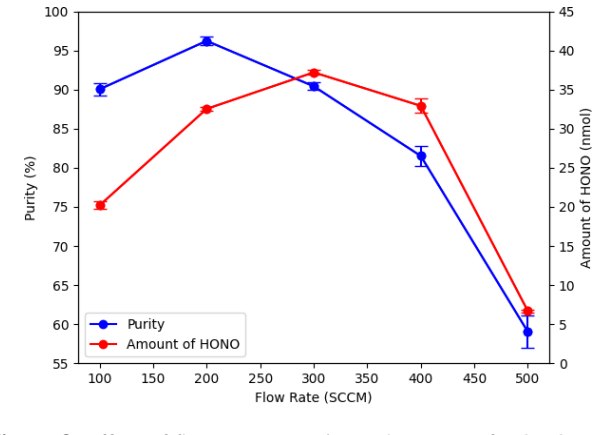
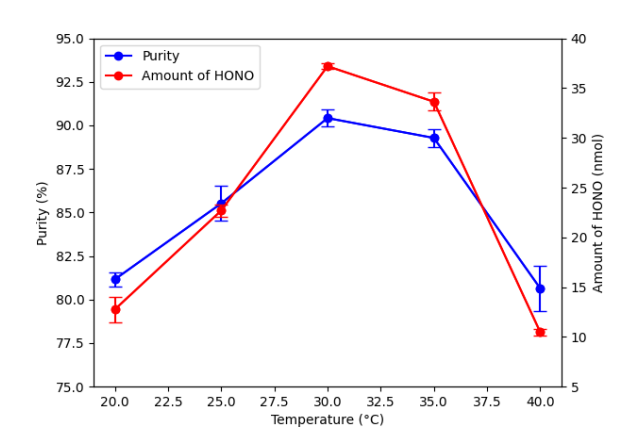
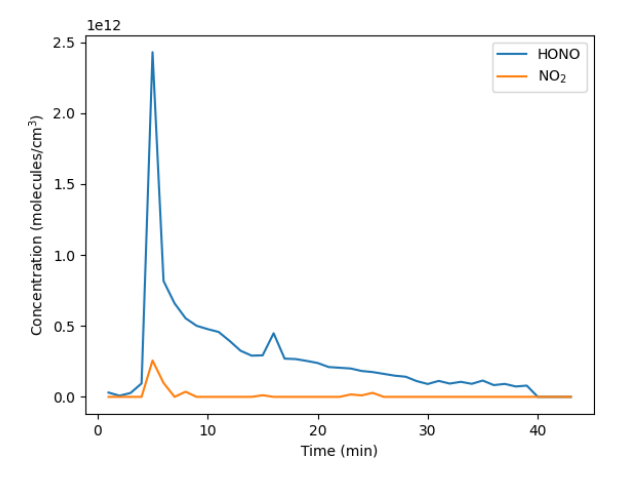


Figure 8. Effect of flow rate on purity and amount of HONO.



**Figure 7.** Effect of reactant bubbler bath temperature on purity and amount of HONO.



**Figure 9.** Concentration of HONO and NO<sub>2</sub> desorbing from the capture bubbler beads using the optimal HONO production method.

water was added to wet the NaNO<sub>2</sub> without fully dissolving it. Specifically, 200 g of NaNO<sub>2</sub> was combined with 20 mL of distilled deionized water. To assess the effect of hydration on HONO production, experiments were conducted under otherwise optimal conditions using either a saturated NaNO<sub>2</sub> solution or dry solid NaNO<sub>2</sub>. The saturated solution yielded HONO at  $44.2 \pm 2.1$ % purity, and the solid NaNO<sub>2</sub> produced a mixture with  $56.4 \pm 2.2$ % purity, both significantly lower than the  $96.2 \pm 0.5$ % purity achieved with the slurry. These findings highlight the critical importance of precisely controlling hydration in the reaction medium.

### 4 Conclusions

This study presents a reproducible, scalable method for generating high-purity HONO relative to NO<sub>2</sub> using a multibubbler system with thermal separation. Through systematic optimization of bubbler temperatures, carrier gas flow, capture duration, and water content, the method achieved HONO purities exceeding 96 % at high and flexible yields. The use of a thermal "catch and release" system not only allows for the decoupling of HONO from interfering NO<sub>2</sub>, but also enables temporary storage of HONO in a condensed phase, offering flexibility in both concentration and timing of release.

This approach overcomes a longstanding limitation in acid displacement generation techniques, where  $NO_2$  coproduction often complicates spectroscopic detection and quantification. When paired with broadband cavity-enhanced absorption spectroscopy (BBCEAS), this generation method supports sensitive, selective, and high-throughput HONO detection, with broad applicability in both laboratory and field-based research. The HONO source can be easily coupled to other detection platforms, including spectroscopic, chemical ionization, or mass spectrometric techniques, and thus enables comparative and intercalibration studies across multiple measurement frameworks.

Beyond BBCEAS calibration, this technique is particularly well-suited for use in environmental chamber experiments. The ability to produce HONO at controlled purity and concentrations enables detailed studies of its role in atmospheric chemistry, including its photolysis into OH radicals, a key driver in tropospheric oxidation. Previous chamber studies such as those at CESAM (Yi et al., 2021) and SAPHIR (Dixneuf et al., 2022) have focused primarily on HONO detection and budget analysis. CESAM has also conducted chamber studies that utilize HONO as the source for OH radical production (Lamkaddam et al., 2019; Picquet-Varrault et al., 2020). We present possibilities for similar chamber studies in a smaller environment, investigating not only HONO abundance, but also its contribution to OH formation and subsequent reaction kinetics within simulated atmospheric environments.

Future applications may include integration with field-deployable HONO sensors, automated sampling systems, or

kinetic studies exploring the influence of HONO on radicaldriven oxidation pathways. Ultimately, this method provides a robust, transferable foundation for investigating HONO chemistry across varied environments by enhancing our capacity to isolate, quantify, and mechanistically understand one of the atmosphere's most influential trace species.

Data availability. Datasets are presented in figures throughout the paper. Raw data from these resources are available on BYU's Scholar's archive (https://scholarsarchive.byu.edu/data/93, Harper et al., 2025).

Author contributions. APH: writing of the original manuscript, data collection and analysis, conceptualization. CEF: project design, conceptualization. ZG and KB: data collection and analysis. RT: project design, conceptualization, and funding acquisition. JCH: supervision and funding acquisition. All authors participated in the review and editing of the manuscript.

Competing interests. The contact author has declared that none of the authors has any competing interests.

Disclaimer. Publisher's note: Copernicus Publications remains neutral with regard to jurisdictional claims made in the text, published maps, institutional affiliations, or any other geographical representation in this paper. While Copernicus Publications makes every effort to include appropriate place names, the final responsibility lies with the authors. Views expressed in the text are those of the authors and do not necessarily reflect the views of the publisher.

Financial support. Student salaries and supplies were provided by the College of Physical and Mathematical Sciences at Brigham Young University. This work was supported by the National Science Foundation (grant no. 2321381). The funder played no role in the study design, data collection, analysis and interpretation of data, or the writing of this manuscript.

Review statement. This paper was edited by Haichao Wang and reviewed by two anonymous referees.

### References

Beine, H., Colussi, A. J., Amoroso, A., Esposito, G., Montagnoli, M., and Hoffmann, M. R.: HONO emissions from snow surfaces, Environ. Res. Lett., 3, 045005, https://doi.org/10.1088/1748-9326/3/4/045005, 2008.

Bongartz, A., Kames, J., Welter, F., and Schurath, U.: Near-UV absorption cross sections and trans/cis equilibrium of nitrous acid, J. Phys. Chem., 95, 1076–1082, https://doi.org/10.1021/j100156a012, 1991.

- Bottorff, B., Reidy, E., Mielke, L., Dusanter, S., and Stevens, P. S.: Development of a laser-photofragmentation laser-induced fluorescence instrument for the detection of nitrous acid and hydroxyl radicals in the atmosphere, Atmos. Meas. Tech., 14, 6039–6056, https://doi.org/10.5194/amt-14-6039-2021, 2021.
- Braman, R. S. and De la Cantera, M. A.: Sublimation sources for nitrous acid and other nitrogen compounds in air, Anal. Chem., 58, 1533–1537, https://doi.org/10.1021/ac00298a059, 1986.
- Burkholder, J. B., Sander, S. P., Abbatt, J. P. D., Barker, J. R., Cappa, C., Crounse, J. D., Dibble, T. S., Huie, R. E., Kolb, C. E., Kurylo, M. J., Orkin, V. L., Percival, C. J., Wilmouth, D. M., and Wine, P. H.: Chemical kinetics and photochemical data for use in atmospheric studies, evaluation number 19, Jet Propulsion Laboratory, Pasadena, CA, NASA JPL Publication 19-5, https://jpldataeval.jpl.nasa.gov/pdf/NASA-JPLEvaluation%2019-5.pdf (last access: 26 November 2025), 2020.
- Cox, R. A. and Derwent, R. G.: The ultraviolet absorption spectrum of gaseous nitrous acid, J. Photochem., 6, 23–34, https://doi.org/10.1016/0047-2670(76)87004-9, 1976b.
- Cox, R. A., Derwent, R. G., and Holt, P. M.: Relative rate constants for the reactions of OH radicals with H<sub>2</sub>, CH<sub>4</sub>, CO, NO and HONO at atmospheric pressure and 296 K, J. Chem. Soc. Faraday Trans. 1, 72, 231–243, https://doi.org/10.1039/F19767202031, 1976a.
- Dixneuf, S., Ruth, A. A., Häseler, R., Brauers, T., Rohrer, F., and Dorn, H.-P.: Detection of nitrous acid in the atmospheric simulation chamber SAPHIR using open-path incoherent broadband cavity-enhanced absorption spectroscopy and extractive long-path absorption photometry, Atmos. Meas. Tech., 15, 945–964, https://doi.org/10.5194/amt-15-945-2022, 2022.
- Duan, J., Qin, M., Ouyang, B., Fang, W., Li, X., Lu, K., Tang, K., Liang, S., Meng, F., Hu, Z., Xie, P., Liu, W., and Häsler, R.: Development of an incoherent broadband cavity-enhanced absorption spectrometer for in situ measurements of HONO and NO<sub>2</sub>, Atmos. Meas. Tech., 11, 4531–4543, https://doi.org/10.5194/amt-11-4531-2018, 2018.
- Dusanter, S., Vimal, D., Stevens, P. S., Volkamer, R., Molina, L. T., Baker, A., Meinardi, S., Blake, D., Sheehy, P., Merten, A., Zhang, R., Zheng, J., Fortner, E. C., Junkermann, W., Dubey, M., Rahn, T., Eichinger, B., Lewandowski, P., Prueger, J., and Holder, H.: Measurements of OH and HO<sub>2</sub> concentrations during the MCMA-2006 field campaign Part 2: Model comparison and radical budget, Atmos. Chem. Phys., 9, 6655–6675, https://doi.org/10.5194/acp-9-6655-2009, 2009.
- Elshorbany, Y., Barnes, I., Becker, K. H., Kleffmann, J., and Wiesen, P.: Sources and cycling of tropospheric hydroxyl radicals an overview, Z. Phys. Chem., 224, 967–987, https://doi.org/10.1524/zpch.2010.6136, 2010.
- Febo, A., Perrino, C., Gherardi, M., and Sparapani, R.: Evaluation of a high-purity and high-stability continuous generation system for nitrous acid, Environ. Sci. Technol., 29, 2390–2395, https://doi.org/10.1021/es00009a035, 1995.
- Finlayson-Pitts, B. J., Wingen, L. M., Sumner, A. L., Syomin, D., and Ramazan, K. A.: The heterogeneous hydrolysis of NO<sub>2</sub> in laboratory systems and in outdoor and indoor atmospheres: an integrated mechanism, Phys. Chem. Chem. Phys., 5, 223–242, https://doi.org/10.1039/b208564j, 2003.

- Flowerday, C. E., Bhardwaj, N., Thalman, R., Asplund, M. C., Sevy, E. T., and Hansen, J. C.: Absorption cross-sections for the 5th and 6th vibrational overtones in a series of short chained alcohols using incoherent broadband cavity enhanced-absorption spectroscopy (IBBCEAS), J. Mol. Spectrosc., 392, 111746, https://doi.org/10.1016/j.jms.2023.111746, 2023a.
- Flowerday, C. E., Thalman, R., Asplund, M. C., and Hansen, J. C.: Broadband cavity-enhanced absorption spectroscopy (BBCEAS) coupled with an interferometer for onband and off-band detection of glyoxal, Toxics, 12, 26, https://doi.org/10.3390/toxics12010026, 2023b.
- Flowerday, C. E., Thalman, R., Asplund, M. C., Badstubner, S. A., Cook, A. K., Lundrigan, P., and Hansen, J. C.: Open path spectroscopic detection of hydroxyl radical: a comparison between broadband cavity-enhanced absorption spectroscopy (BBCEAS) and BBCEAS coupled with a Fabry–Pérot interferometer (BBCEAS-FP), Anal. Chem., 97, 11831–11839, https://doi.org/10.1021/acs.analchem.5c01515, 2025.
- Gherman, T., Venables, D. S., Vaughan, S., Orphal, J., and Ruth, A. A.: Incoherent broadband cavity-enhanced absorption spectroscopy in the near-ultraviolet: application to HONO and  $NO_2$ , Environ. Sci. Technol., 42, 890–895, https://doi.org/10.1021/es0716913, 2008.
- Gingerysty, N. J. and Osthoff, H. D.: A compact, high-purity source of HONO validated by Fourier transform infrared and thermal-dissociation cavity ring-down spectroscopy, Atmos. Meas. Tech., 13, 4159–4167, https://doi.org/10.5194/amt-13-4159-2020, 2020.
- Gutzwiller, L., Arens, F., Baltensperger, U., Gäggeler, H. W., and Ammann, M.: Significance of semivolatile diesel exhaust organics for secondary HONO formation, Environ. Sci. Technol., 36, 677–682, https://doi.org/10.1021/es015673b, 2002.
- Harper, A. P., Flowerday, C. E., Giauque, Z., Brewster, K., Thalman, R., and Hansen, J. C.: High-purity nitrous acid (HONO) generation and quantification using broadband cavity-enhanced absorption spectroscopy (BBCEAS), BYU ScholarArchive [data set], https://scholarsarchive.byu.edu/data/93 (last access: 10 November 2025), 2025.
- Heland, J., Kleffmann, J., Kurtenbach, R., and Wiesen, P.: A new instrument to measure gaseous nitrous acid (HONO) in the atmosphere, Environ. Sci. Technol., 35, 3207–3212, https://doi.org/10.1021/es000303t, 2001.
- Honrath, R. E., Lu, Y., Peterson, M. C., Dibb, J. E., Arsenault, M. A., Cullen, N. J., and Steffen, K.: Vertical fluxes of NO<sub>x</sub>, HONO, and HNO<sub>3</sub> above the snowpack at Summit, Greenland, Atmos. Environ., 36, 2629–2640, https://doi.org/10.1016/S1352-2310(02)00132-2, 2002.
- Jordan, N. and Osthoff, H. D.: Quantification of nitrous acid (HONO) and nitrogen dioxide (NO<sub>2</sub>) in ambient air by broadband cavity-enhanced absorption spectroscopy (IBBCEAS) between 361 and 388 nm, Atmos. Meas. Tech., 13, 273–285, https://doi.org/10.5194/amt-13-273-2020, 2020.
- Kanda, Y. and Taira, M.: Chemiluminescent method for continuous monitoring of nitrous acid in ambient air, Anal. Chem., 62, 2084– 2087, https://doi.org/10.1021/ac00218a007, 1990.
- King, G. W. and Moule, D.: The ultraviolet absorption spectrum of nitrous acid in the vapor state, Can. J. Chem., 40, 2057–2065, https://doi.org/10.1139/v62-316, 1962.

- Kleffmann, J.: Daytime sources of nitrous acid (HONO) in the atmospheric boundary layer, Chem. Phys. Chem., 8, 1137–1144, https://doi.org/10.1002/cphc.200700016, 2007.
- Kurtenbach, R., Becker, K. H., Gomes, J. A. G., Kleffman, J., Lörzer, J. C., Spittler, M., Wiesen, P., Ackermann, R., Geyer, A., and Platt, U.: Investigations of emissions and heterogeneous formation of HONO in a road traffic tunnel, Atmos. Environ., 35, 3385–3394, https://doi.org/10.1016/S1352-2310(01)00138-8, 2001.
- Lamkaddam, H., Gratien, A., Ropion, M., Pangui, E., and Doussin, J. F.: Kinetic study of the temperature dependence of OHinitiated oxidation of n-dodecane, J. Phys. Chem. A, 123, 9462– 9468, https://doi.org/10.1021/acs.jpca.9b07704, 2019.
- Lao, M., Crilley, L. R., Salehpoor, L., Furlani, T. C., Bourgeois, I., Neuman, J. A., Rollins, A. W., Veres, P. R., Washenfelder, R. A., Womack, C. C., Young, C. J., and VandenBoer, T. C.: A portable, robust, stable, and tunable calibration source for gasphase nitrous acid (HONO), Atmos. Meas. Tech., 13, 5873–5890, https://doi.org/10.5194/amt-13-5873-2020, 2020.
- Michoud, V., Colomb, A., Borbon, A., Miet, K., Beekmann, M., Camredon, M., Aumont, B., Perrier, S., Zapf, P., Siour, G., Ait-Helal, W., Afif, C., Kukui, A., Furger, M., Dupont, J. C., Haeffelin, M., and Doussin, J. F.: Study of the unknown HONO day-time source at a European suburban site during the MEGAPOLI summer and winter field campaigns, Atmos. Chem. Phys., 14, 2805–2822, https://doi.org/10.5194/acp-14-2805-2014, 2014.
- Ning, C. L. and Pfab, J.: Generation and 355 nm laser photodissociation of nitrous acid (HONO) and HONO–water clusters, J. Phys. Chem. A, 101, 6008–6014, https://doi.org/10.1021/jp9711712, 1997
- O'Neil, M. J., Heckelman, P. E., Dobbelaar, P. H., Roman, K. J., Kenny, C. M., and Karaffa, L. S.: The Merck Index: an encyclopedia of chemicals, drugs, and biologicals, 15th edn., The Royal Society of Chemistry, Cambridge, UK, ISBN 9781849736701, 2013.
- Picquet-Varrault, B., Suarez-Bertoa, R., Duncianu, M., Cazaunau, M., Pangui, E., David, M., and Doussin, J.-F.: Photolysis and oxidation by OH radicals of two carbonyl nitrates: 4-nitrooxy-2-butanone and 5-nitrooxy-2-pentanone, Atmos. Chem. Phys., 20, 487–498, https://doi.org/10.5194/acp-20-487-2020, 2020.
- Pitts, J. N., Biermann, H. W., Winer, A. M., and Tuazon, E. C.: Spectroscopic identification and measurement of gaseous nitrous acid in dilute auto exhaust, Atmos. Environ., 18, 847–854, https://doi.org/10.1016/0004-6981(84)90270-1, 1984.
- Reed, C., Brumby, C. A., Crilley, L. R., Kramer, L. J., Bloss, W. J., Seakins, P. W., Lee, J. D., and Carpenter, L. J.: HONO measurement by differential photolysis, Atmos. Meas. Tech., 9, 2483– 2495, https://doi.org/10.5194/amt-9-2483-2016, 2016.
- Ren, X., Harder, H., Martinez, M., Lesher, R. L., Oliger, A., Simpas, J. B., Brune, W. H., Schwab, J. J., Demerjian, K., He, Y., Zhou, X. L., and Gao, H.: OH and HO<sub>2</sub> chemistry in the urban atmosphere of New York City, Atmos. Environ., 37, 3639–3651, https://doi.org/10.1016/s1352-2310(03)00459-x, 2003.
- Ren, X., Brune, W. H., Mao, J., Mitchell, M. J., Lesher, R. L., Simpas, J. B., Metcalf, A. R., Schwab, J. J., Cai, C., Ii, Y., Demerjian, K., Felton, D., Boynton, G., Adams, A., Perry, J., He, Y., Zhou, X., and Hou, J.: Behavior of OH and HO<sub>2</sub> in the winter atmosphere in New York City, Atmos. Environ., 40, 252–263, https://doi.org/10.1016/j.atmosenv.2005.11.073, 2006.

- Stockwell, W. R. and Calvert, J. G.: The near ultraviolet absorption spectrum of gaseous HONO and N<sub>2</sub>O<sub>3</sub>, J. Photochem., 8, 193–203, https://doi.org/10.1016/0047-2670(78)80019-7, 1978.
- Stutz, J., Kim, E. S., Platt, U., Bruno, P., Perrino, C., and Febo, A.: UV-visible absorption cross sections of nitrous acid, J. Geophys. Res., 105, 14585–14592, https://doi.org/10.1029/2000JD900003, 2000.
- Su, H., Cheng, Y., Oswald, R., Behrendt, T., Trebs, I., Meixner, F. X., Andreae, M. O., Cheng, P., Zhang, Y., and Pöschl, U.: Soil nitrite as a source of atmospheric HONO and OH radicals, Science, 333, 1616–1618, https://doi.org/10.1126/science.1207687, 2011.
- Taira, M. and Kanda, Y.: Continuous generation system for low-concentration gaseous nitrous acid, Anal. Chem., 62, 630–633, https://doi.org/10.1021/ac00205a018, 1990.
- Thalman, R. and Volkamer, R.: Inherent calibration of a blue LED-CE-DOAS instrument to measure iodine oxide, glyoxal, methyl glyoxal, nitrogen dioxide, water vapour and aerosol extinction in open cavity mode, Atmos. Meas. Tech., 3, 1797–1814, https://doi.org/10.5194/amt-3-1797-2010, 2010.
- Thalman, R., Bhardwaj, N., Flowerday, C. E., and Hansen, J. C.: Detection of sulfur dioxide by broadband cavityenhanced absorption spectroscopy (BBCEAS), Sensors, 22, 2626, https://doi.org/10.3390/s22072626, 2022.
- Vandaele, A. C., Hermans, C., Simon, P. C., Carleer, M. R., Colin, R., Fally, S., Merienne, M. F., Jenouvrier, A., and Coquart, B.: Measurements of the NO<sub>2</sub> absorption cross-section from 42 000 cm<sup>-1</sup> to 10 000 cm<sup>-1</sup> (238–1000 nm) at 220 K and 294 K, J. Quant. Spectrosc. Ra., 59, 171–184, https://doi.org/10.1016/s0022-4073(97)00168-4, 1998.
- Villena, G. and Kleffmann, J.: A source for the continuous generation of pure and quantifiable HONO mixtures, Atmos. Meas. Tech., 15, 627–637, https://doi.org/10.5194/amt-15-627-2022, 2022.
- von der Heyden, L., Wißdorf, W., Kurtenbach, R., and Kleffmann, J.: A relaxed eddy accumulation (REA) LOPAP system for flux measurements of nitrous acid (HONO), Atmos. Meas. Tech., 15, 1983–2000, https://doi.org/10.5194/amt-15-1983-2022, 2022.
- Washenfelder, R. A., Attwood, A. R., Flores, J. M., Zarzana, K. J., Rudich, Y., and Brown, S. S.: Broadband cavity-enhanced absorption spectroscopy in the ultraviolet spectral region for measurements of nitrogen dioxide and formaldehyde, Atmos. Meas. Tech., 9, 41–52, https://doi.org/10.5194/amt-9-41-2016, 2016.
- Wu, T., Chen, W., Fertein, E., Cazier, F., Dewaele, D., and Gao, X.: Development of an open-path incoherent broadband cavityenhanced spectroscopy-based instrument for simultaneous measurement of HONO and NO<sub>2</sub> in ambient air, Appl. Phys. B, 106, 501–509, https://doi.org/10.1007/s00340-011-4818-3, 2012.
- Wu, T., Zha, Q., Chen, W., Xu, Z., Wang, T., and He, X.: Development and deployment of a cavity enhanced UV-LED spectrometer for measurements of atmospheric HONO and NO<sub>2</sub> in Hong Kong, Atmos. Environ., 95, 544–551, https://doi.org/10.1016/j.atmosenv.2014.07.016, 2014.
- Xu, Z., Wang, T., Wu, J., Xue, L., Chan, J., Zha, Q., Zhou, S., Louie, P. K. K., and Luk, C. W. Y.: Nitrous acid (HONO) in a polluted subtropical atmosphere: seasonal variability, direct vehicle emissions and heterogeneous production at ground surface, Atmos. Environ., 106, 100–109, https://doi.org/10.1016/j.atmosenv.2015.01.061, 2015.

Yi, H., Cazaunau, M., Gratien, A., Michoud, V., Pangui, E., Doussin, J.-F., and Chen, W.: Intercomparison of IBBCEAS, NitroMAC and FTIR analyses for HONO, NO<sub>2</sub> and CH<sub>2</sub>O measurements during the reaction of NO<sub>2</sub> with H<sub>2</sub>O vapour in the simulation chamber CESAM, Atmos. Meas. Tech., 14, 5701–5715, https://doi.org/10.5194/amt-14-5701-2021, 2021.